Processing and Application of Ceramics 10 [4] (2016) 235–241
DOI: 10.2298/PAC1604235G



# Heating rate dependence of anatase to rutile transformation

Pietro Galizia[1,2,*], Giovanni Maizza[2], Carmen Galassi[1]

[1]*CNR-ISTEC National Research Council of Italy - Institute of Science and Technology for Ceramics, Faenza (RA), 48018 Italy*
[2]*Polytechnic of Turin, Department of Applied Science and Technology, Torino (TO), 10129 Italy*

Received 22 August 2016; Received in revised form 28 October 2016; Accepted 16 November 2016

## Abstract

*Commercial titania powders were calcined in order to investigate the influence of the heating history on the thermally stable phase (rutile). Temperatures from 620 to 700 °C and heating rates from 50 to 300 °C/h were used in order to evaluate their influence on the kinetics of transformation and microstructure evolution. The quantitative analysis of anatase-rutile mixtures based on X-ray diffraction intensities was performed. The results were plotted as cumulative transformation rate vs. cumulative coarsening rate in order to address the heating history of the anatase to rutile transformation. As the main result it was found that the amount of anatase transformed into rutile increases with increasing heating rate at fixed soaking time and temperature of calcination. Through linear extrapolation of experimental data obtained from the calcined commercial titania Degussa P25, it was found that 83 nm for the rutile crystallite size is the lowest limit needed for getting 100% of rutile powders. A substantial improvement in the anatase to rutile kinetic transformation was achieved after pressing the starting powders in order to exploit the interface nucleation.*

***Keywords:*** *titania, calcination, X-ray diffraction, polymorphic phase transformation kinetic*

## I. Introduction

Titanium dioxide ($TiO_2$) is a very well-known dielectric material in each of its naturally occurring polymorphic phases: anatase (tetragonal *I4/amd*), brookite (orthorhombic *Pcab*), and rutile (tetragonal *P42/mnm*) [1]. Since 1941 the rutile, with a dielectric constant of around 100–150 (at room temperature and in the range of 100 Hz to 1 MHz) [2,3] showed the highest values [4,5]. Therefore a great quantity of research has been brought out to study the preparation, anomalous behaviour and potential applications of this material [6–12]. Today, the titania powder is mainly used in the anatase form in applications such as solar energy storage cells [13,14], catalysts and degradation of organic compounds [15–20]. Rutile does not show the high photoreactivity of anatase [21] and is used mainly for pigments due to its effective high light scattering [22] and also for its large static dielectric constant [19,23]. Moreover there are many researches that have demonstrated rutile's photocatalytic activity similar to anatase when the crystal size of both phases was comparable [24]. This goal was achieved when the rutile was not prepared as thermally stable phase as reported by Eraiah *et al.* [25].

The Degussa P25 $TiO_2$ (P25) is a largely used commercial material supplied as a powder mixture of anatase (major) and rutile and amorphous (minor) phases with different ratios depending on the batch [26]. The powder is a mixture of anatase and rutile in the ratio about 3:1, and rutile is present as separate phase and does not exist on the surface of the individual particles of anatase [27]. The existence of two different phases, their unknown precise amount, and the nanometric sized particles may give some problems during the synthesis, shaping and sintering of ceramic materials. In particular, the presence of nanosized particles, especially when mixed with micronic powders and high density difference between anatase (size: 24.5 nm; bulk density: 3.893 g/cm$^3$, ICDD-PDF-2 code number 00-021-1272) and rutile (size: 44.1 nm; bulk density: 4.25 g/cm$^3$ ICDD-PDF-2 code number 00-021-1276), as in the case of this commercial powder, is worthy of further investigations. In fact, the presence of nanopar-

*Corresponding author: tel: +39 0546699777,
e-mail: *pietro.galizia@istec.cnr.it* (P. Galizia)
e-mail: *giovanni.maizza@polito.it* (G. Maizza)
e-mail: *carmen.galassi@istec.cnr.it* (C. Galassi)

ticles with high surface area contributes non-negligibly to the chemical potential by changing the activation energy for the phase transformation. For example, in the phase diagrams taken into consideration, there is a significant difference from the value reported by Dachille *et al.* [28], which plotted the extrapolations to atmospheric pressure of the anatase-rutile boundaries intersecting the temperature axis at 605 °C, in comparison to the anatase-rutile phase transition temperature reported more recently by Sun *et al.* [25] and fixed at 780 °C. Further, the phase stability, that, at room temperature and for macro-crystalline powders, is higher for rutile than for anatase, reverses when particle size becomes less than 10–15 nm [29–31]. Thus, by varying the initial size of $TiO_2$ nanoparticles the phase transformation reaction path changes, both in terms of transition onset point and growth rate. The significant change of transformation rate and activation energy (about 165.6 kJ/mol and over 330 kJ/mol, respectively, for rutile nucleation, within nanocrystalline anatase particles and coarse ones [32,33]) result into a transition temperature that can vary from 400 °C to 1200 °C [25,34,35].

The anatase to rutile transformation occurs with a coarsening mechanism. On the other hand, the rutile nucleation is dominated by surface nucleation (surface nucleation > interface nucleation > bulk nucleation) [36]. This transformation can be regarded as reconstructive phase transformation, which requires repositioning of both Ti cations and change in the oxygen arrangement. This implies that at the interface of two anatase particles atomic migration is the primary driving force for the formation and growth of rutile nuclei. The migration is strongly dependent on potential driving forces for anatase to rutile transition that decreases at increasing anatase particle size and correlated surface area. The transition driving force is due to the atoms in the defect sites which have higher energy than those in the main lattice and can favourably act as nucleation sites for the rutile phase formation at the surface of anatase crystallites. Thus, rutile nuclei keep consuming anatase particles from their interface until its total free energy becomes equal to or smaller than that of anatase. Therefore, it is easier to overcome the energy barrier to start the transformation of anatase to rutile with finer particles due to their higher free surface area and concentration of anatase particle-particle contact points. Since the anatase particle-particle boundaries are the nucleation sites for the polymorphic phase transition, the phase transformation rate of nanocrystalline anatase can be related to the "concentration" of anatase particles [32]. The kinetics of the anatase-to-rutile phase transformation was investigated by several researchers (as well summarized by Zhang and Banfield [32]) and studied as a function of temperature, pressure, particle size, additive/dopant, hydrothermal condition but the influence of heating rate during the transformation has not been emphasized.

This work aims to find the best calcination cycle - in air and with "natural" cooling in oven (without quenching treatment) - in order to achieve the highest transformation rate of the anatase into rutile in commercial P25 powder, while keeping the crystallite size and particle size distribution, respectively, as low and as uniform as possible [8], and to improve the quality of the calcined P25 powder for applications as a filler or precursor for functional ceramic composites [37,38]. Li *et al.* [3] observed that the particle sizes become larger and non-uniform with the increase of the annealing temperature. Therefore temperature and time of calcination must be kept as low as possible. So the approach is to increase the heating rate in order to boost the non-equilibrium transition from anatase to rutile by exploiting the higher surface areas, so as to reduce the activation energy needed for transition [36]; the requested energy will be available if the surface area and particle radius of anatase particles, respectively, are as high and as low as possible when the onset temperature (related to the particle size at the starting point) is reached. The full transformation was achieved by shaping the powders in a compacted green body in order to increase the contact points between the particles of anatase. In this way the coarsening mechanism was exploited increasing the "concentration" of anatase particles, while keeping the heating rate as high as possible.

We believe that the control of a mild thermal treatment of commercial P25 will allow to reduce dispersity and aggregation of rutile particles with nanometre size.

## II. Experimental procedure

All phase transformation experiments were carried out under normal pressure (1 atm) in a Nannetti Klin FCN 16 furnace controlled using an Ero-Electronic PKP controller. Three samples (#1, #2, #3) used in the kinetic experiments were based on ~20 g $TiO_2$ (Degussa P25) powders. For the fourth sample (#4), 4 g of $TiO_2$ (Degussa P25) powder was subjected to cold linear pressing at 70 MPa to produce 30 mm diameter, 3 mm thick disk. Isostatic pressing at 300 MPa was applied to the disk to obtain green homogeneous $TiO_2$ body. All the samples were fired by setting the heat treatment cycles reported in Table 1. From one cycle to the following one the samples were cooled down to room temperature by free cooling of the furnace. In Table 1, the cooling times ($t_c$) which passed from the calcination temperature to 605 °C, which is the equilibrium temperature at atmospheric pressure reported by Dachille *et al.* [28], are reported. The crystallite's growth and relative phase contents for anatase and rutile were quantitatively evaluated by Powder X-Ray Diffraction (PXRD) analysis by using Bruker D8 Advanced X-ray diffractometer ($\theta$–$\theta$) with a LYNXEYE detector. PXRD patterns were recorded with Cu $K_\alpha$ radiation in the range $0° \leq 2\theta \leq 60°$ which includes most of the main anatase and rutile diffraction peaks. The scan speed and point intervals were kept at 2.4°/min and 0.02°, respectively.

**Table 1. Heating treatments performed on samples of Degussa P25 powder**

| Sample | Step, $i$ | Heating rate, $q$ [°C/h] | Calcination temperature, $T$ [°C] | Permanence time, $t$ [h] | Cooling time, $t_c$ [min] |
|---|---|---|---|---|---|
| #1 | 1 | 100 | 620 | 0.5 | 1 |
| | 2 | 100 | 640 | 1 | 3 |
| | 3 | 100 | 640 | 5 | 3 |
| | 4 | 100 | 620 | 50 | 1 |
| | 5 | 100 | 700 | 1 | 7 |
| #2 | 1 | 200 | 680 | 1 | 5 |
| | 2 | 100 | 700 | 1 | 7 |
| #3 | 1 | 300 | 700 | 1 | 7 |
| #4 | 1 | 300 | 700 | 1 | 7 |

## III. Results

Figure 1 shows the PXRD patterns of P25 samples. All peaks belong to the anatase and rutile phases and no other phase is detected within the X-ray detection limit. The average crystallite sizes ($D_A$ for anatase and $D_R$ for rutile) were calculated by Scherrer's formula, $D = k\lambda/\beta\cos\theta$, based on the precise $2\theta$ positions and full width at half maxima ($\beta$) of the diffraction peaks with background-subtracted and Lorentzian correction of 0.037° on $\beta$ due to the instrumental peak broadening. The values of $\beta$ and $\theta$ are taken for anatase crystal planes (101) and rutile one (110). The shape factor ($k$) and the X-ray wavelength ($\lambda$) were fixed at 0.9 and 0.15418 nm, respectively. Following this formula, the XRD calculation does not give the true average crystal size but an apparent one, which, anyway, depends on the first.

The phase composition is calculated by the Spurr and Meyer's equation formula [39]:

$$W_R = \frac{A_R}{A_0} = \frac{A_R}{0.884A_A + A_R} \quad (1)$$

where $W_R$ is the rutile weight fraction, $A_A$ and $A_R$ are integrated diffraction peak intensities (after background-subtraction) of the strongest peaks of anatase (101) and rutile (110) fitted by Pearson VII curves, respectively, and $A_0$ is the total integrated 101 and 110 peaks intensity. It has been supposed that the possible amount of amorphous phase [26,40], about 9% [41], corresponds to anatase particles with crystallites smaller than 30 Å. The measured particle sizes and percentage amount of calculated phases for each heat treatment step are shown in Table 2. The commercial powder $TiO_2$ (Degussa P25) that has an average size of about 30 nm, was also characterized as supplied for comparison, and used as standard for initial composition.

## IV. Discussion

The measured average crystallite sizes and the percentage amount of detected phases for each heat treatment (data reported in Table 2) were processed in order to evaluate the role of heating rate and the thermal history. For this purpose in Fig. 2 the cumulative trans-

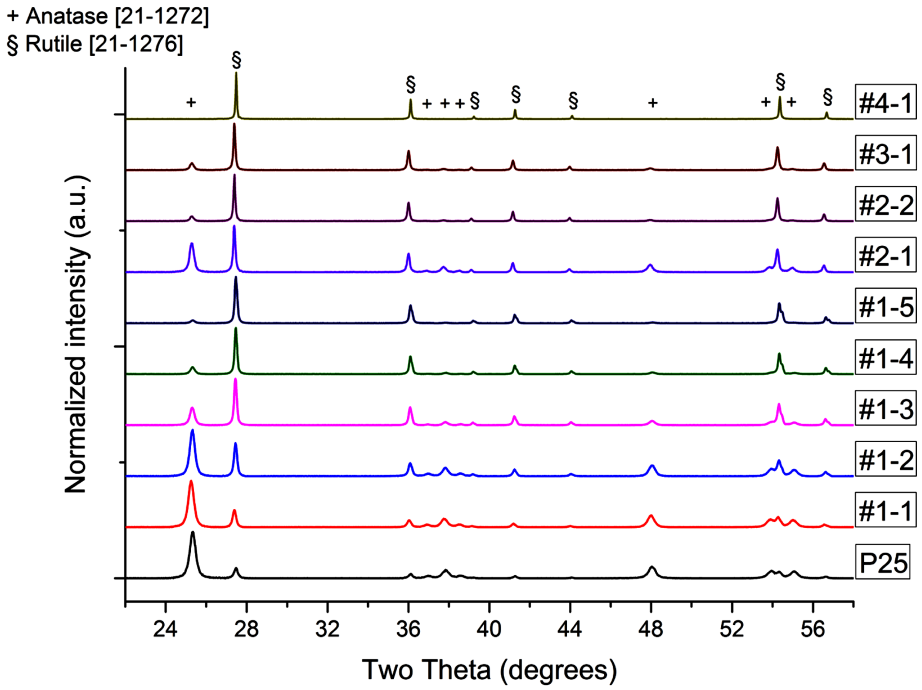


**Figure 1. Normalized PXRD patterns (the first and the second number denote sample and step *i*, respectively)**

**Table 2. The measured particle sizes and percentage amount of calculated phases**

| Sample | Step, $i$ | $W_R$ [wt./wt.] | $D_R$ [nm] | $D_A$ [nm] | Slope [$10^{-3}$ nm$^{-1}$] |
|---|---|---|---|---|---|
| P25 | 0 | 0.15 | 36 | 24 | - |
| #1 | 1 | 0.22 | 42 | 26 | 11±1 |
| | 2 | 0.35 | 53 | 29 | 11±2 |
| | 3 | 0.63 | 71 | 32 | 13±2 |
| | 4 | 0.82 | 87 | 37 | 11±2 |
| | 5 | 0.91 | 94 | 41 | 11±2 |
| #2 | 1 | 0.54 | 61 | 30 | 17±1 |
| | 2 | 0.88 | 89 | 38 | 16±2 |
| #3 | 1 | 0.86 | 75 | 35 | 18±1 |
| #4 | 1 | 1 | >100 | - | - |

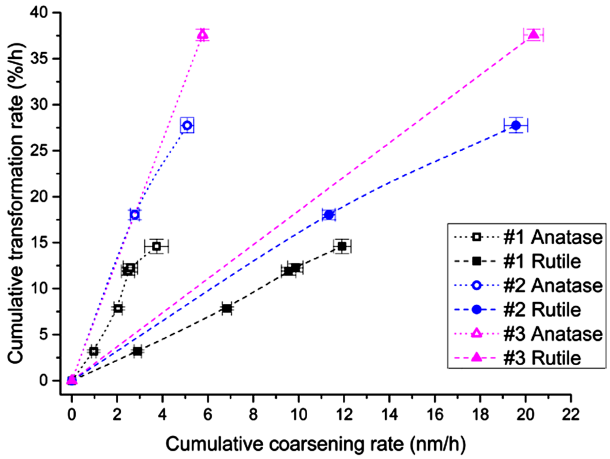


**Figure 2. Plot showing the correlation between transformation rate and coarsening rate of anatase and rutile for each step of kinetic experiments run at the condition reported in Table 1**

formation rate, $\dot{\alpha}$, and the cumulative coarsening rate, $\dot{d}$, were approximated and plotted, respectively, as follows:

$$\dot{\alpha} = \sum_{i=0}^{n} \left| W_{A/R_{i+1}} - W_{A/R_i} \right| / t_{i+1} \quad (2)$$

$$\dot{d} = \sum_{i=0}^{n} \left| D_{A/R_{i+1}} - D_{A/R_i} \right| / t_{i+1} \quad (3)$$

where $t_i$ is the overall time of the step $i$ calculated as the sum of the time spent to reach the calcination temperature from 465 °C [31], plus the soaking time, plus the time of free cooling ($t_c$) down to 605 °C [28].

From the plot (Fig. 2) it can be seen that the slope of anatase curves is always higher than rutile one and this is coherent with the coarsening mechanism. Anatase coarsening rate is always lower than rutile's one. This means that adjacent anatase crystallites tend to transform to rutile rather than to coarsen, so even if the anatase crystallite sizes increase during the treatment, this phenomenon is hidden or decremented by the transformation to rutile which consumes the anatase particles. This was shown by Gribb and Banfield [29] who found partially reacted anatase particles. So, both anatase and rutile particle sizes increase with the increase in temperature, but the growth rate is different. The rutile has much higher growth rate than anatase.

The curves, plotted in Fig. 2, confirm also the effect of the starting crystallite size and the "concentration" of anatase particles on the kinetics of the anatase-to-rutile phase transformation. Considering the last step of the curves #1 and #2 – the same heating rate (Table 1), with different initial $D_{A_i}$ and $W_{A_i}$ (Table 2) – the slope $(W_{R_{i+1}} - W_{R_i})/(D_{R_{i+1}} - D_{R_i})$ increases from about 0.011 nm$^{-1}$ to 0.016 nm$^{-1}$, respectively. Nevertheless, it is not possible to distinguish the specific contributions

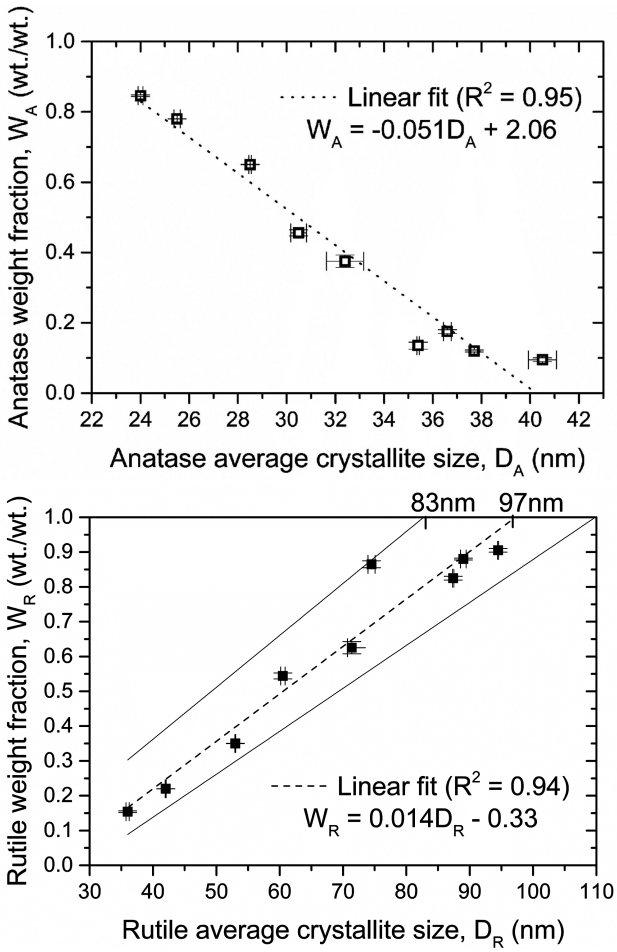


**Figure 3. Weight fraction vs. average crystallite size for anatase (top) and rutile (bottom)**

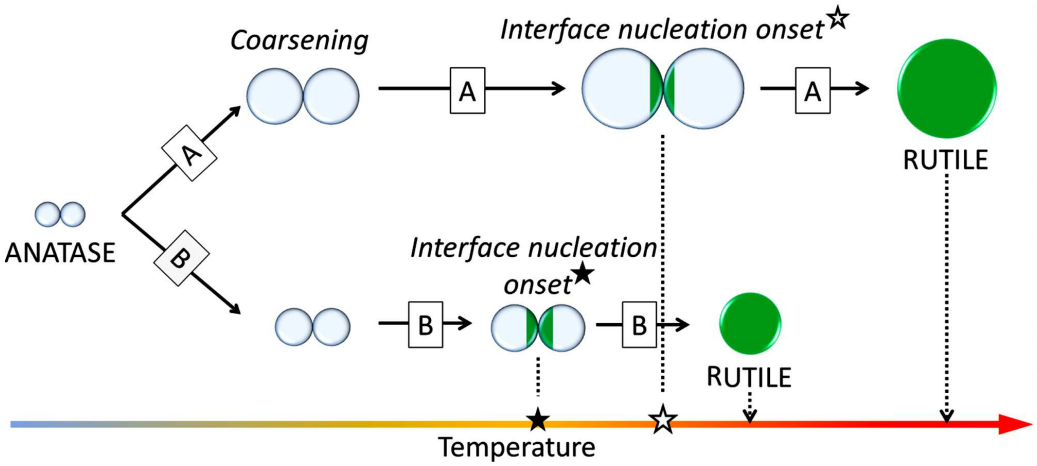


**Figure 4. Diagram showing steps involved in the phase transformation of nanocrystalline anatase particles over lower heating rate (A) and over higher heating rate (B)**

of $D_{A_i}$ and $W_{A_i}$. From the data reported in Table 2 it seems there is a close correlation between $D_{A/R}$ and $W_{A/R}$ which is not strongly influenced by the thermal history. In fact, a linear correlation between them (with a quite high $R^2$ = 0.95 and 0.94 for the anatase and rutile, respectively) was found (Fig. 3). According to the model proposed by Zhang and Bandfield [32] the kinetic of anatase to rutile transformation is a function of the numeric fraction of anatase particles and thus it is directly proportional to $W_A$ and inversely proportional to $(D_A/2)^3$. So, in order to boost the kinetics of transformation of a given anatase and rutile nanopowder mixture, it is fundamental to supply enough thermal energy to the system in short time. This suppresses the coarsening of adjacent anatase particles [42] and their stabilization at higher temperatures. In fact, the highest slope of 0.019 $nm^{-1}$ was achieved at the highest heating rate starting from the powders characterized by the highest value of $W_A$ and the lowest $D_A$. The above discussed heating rate role in the anatase to rutile transformation is summarized as graphical kinetic model in Fig. 4.

The coarsening mechanism was also confirmed and exploited by pressing the starting powder into a disk in order to increase the anatase-anatase contact-points. In this way the anatase to rutile mechanism was significantly improved achieving the full transformation to rutile.

According to the linear correlation between $D_R$ and $W_R$ ($W_R = 0.014D_R - 0.33$) and the results achieved by increasing the heating rate and anatase-anatase contact-points, it should not be possible to get 100% of rutile powders characterized by a $D_R$ smaller than 97 ± 14 nm.

## V. Conclusions

The influence of heating rate and thermal history on the anatase to rutile transformation and crystallite size of commercial $TiO_2$ (Degussa P25) powder was studied. The enhanced anatase to rutile transformation, as a consequence of the increase of the heating rate, results into the highest ratio of rutile weight percentage (86 wt.%) to its crystallite size (75 nm). At the same heat treatment, the full transformation was achieved by increasing the anatase-anatase contact-points. A theoretical lower threshold on the rutile crystallite size was found. It is not possible to get 100% of rutile particles with average crystallite size lower than 83 nm by firing $TiO_2$ Degussa P25 powders.

**Acknowledgements:** The authors thank A. Piancastelli (CNR-ISTEC) for the XRD spectra. Financial support from the "Progetto Premiale - Tecnologie e Sistemi Innovativi per la Fabbrica del Futuro e Made in Italy" project funded by MIUR (Italian Ministry of Education, University and Research) is gratefully acknowledged.

## References

1. A. Thilagam, D.J. Simpson, A.R. Gerson, "A first-principles study of the dielectric properties of $TiO_2$ polymorphs", *J. Phys. Condens. Matter*, **23** (2011) 1–13.
2. S. Marinel, D.H. Choi, R. Heuguent, D. Agrawal, M. Lanagan, "Broadband dielectric characterization of $TiO_2$ ceramics sintered through microwave and conventional processes", *Ceram. Int.*, **39** (2013) 299–306.
3. L.D. Zhang, H.F. Zhang, G.Z. Wang, C.M. Mo, Y. Zhang, "Dielectric behaviour of nano-$TiO_2$ bulks", *Phys. Stat. Sol.*, **157** (1996) 483–491.
4. B. Jaffe, W.R. Cook, H. Jaffe, *Piezoelectric ceramics*, Chapter 1, Academic Press, London and New York, 1971.
5. X.-S. Ye, Z.-G. Xiao, D.-S. Lin, S.-Y. Huang, Y.-H. Man, "Experimental investigation on the dielectric behavior of nanostructured rutile-phase titania", *Mater. Sci. Eng. B*, **74** (2000) 133–136.
6. H. Gleiter, "Nanocrystalline materials", *Prog. Mater. Sci.*, **33** (1989) 223–315.
7. G.A. Samara, P.S. Peercy, "Pressure and temperature dependence of the static dielectric constants and Raman spectra of $TiO_2$ (rutile)", *Phys. Rev. B*, **7** (1973)

1131–1148.
8. A. Wypych, I. Bobowska, M. Tracz, A. Opasinska, S. Kadlubowski, A. Krzywania-Kaliszewska, J. Grobelny, P. Wojciechowski, "Dielectric properties and characterisation of titanium dioxide obtained by different chemistry methods", *J. Nanomater.*, **2014** (2014) 1–9.
9. L.-X. Pang, H. Wang, D. Zhou, X. Yao, "Low-temperature sintering and microwave dielectric properties of $TiO_2$-based LTCC materials", *J. Mater. Sci.*, **21** (2010) 1285–1292.
10. M. Crippa, A. Bianchi, D. Cristofori, M. D'Arienzo, F. Merletti, F. Morazzoni, R. Scotti, R. Simonutti, "High dielectric constant rutile-polystyrene composite with enhanced percolative threshold", *J. Mater. Chem. C*, **1** (2013) 484–492.
11. X. Huang, Z. Pu, L. Tong, Z. Wang, X. Liu, "Preparation and dielectric properties of surface modified $TiO_2$/PEN composite films with high thermal stability and flexibility", *J. Mater. Sci.*, **23** (2012) 2089–2097.
12. R.P. Ortiz, A. Facchetti, T.J. Marks, "High-k organic, inorganic, and hybrid dielectrics for low-voltage organic fieldeffect transistors", *Chem. Rev.*, **110** (2010) 205–239.
13. A. Hagfeldt, M. Gratzel, "Molecular photovoltaics", *Acc. Chem. Res.*, **33** (2000) 269–277.
14. N. Serpone, "A decade of heterogeneous photocatalysis in our laboratory: pure and applied studies in energy production and environmental detoxification", *Res. Chem. Intermed.*, **20** (1994) 953–992.
15. M.A. Fox, M.T. Dulay, "Heterogeneous photocatalysis", *Chem. Rev.*, **93** (1993) 341–357.
16. R.G. Aditi, B.F. Julio, "Methylation of phenol over Degussa P25 $TiO_2$", *J. Mol. Catal. A: Chem.*, **226** (2005) 171–177.
17. W. Chiron, A. Fernandes-Alba, A. Rodriguez, E. Garcia-Calvo, "Pesticide chemical oxidation: state-of-the-art", *Water Res.*, **34** (2000) 366–377.
18. M.A. Anderson, "Applications in photocatalytic purification of air", *Stud. Surf. Sci. Catal.*, **103** (1997) 445–461.
19. M. Schmidt , E. Weitz, F. M. Geiger, "Interaction of the indoor air pollutant acetone with Degussa P25 $TiO_2$ studied by chemical ionization mass spectrometry", *Langmuir*, **22** (2006) 9642–9650.
20. D. Gumy, C. Morais, P. Bowen, C. Pulgarin, S. Giraldo, R. Hajdu, J. Kiwi, "Catalytic activity of commercial of $TiO_2$ powders for the abatement of the bacteria (E. coli) under solar simulated light: Influence of the isoelectric point", *Appl. Catal. B: Environ.*, **63** (2006) 76–84.
21. T. Luttrell, S. Halpegamage, J. Tao, A. Kramer, E. Sutter, M. Batzill, "Why is anatase a better photocatalyst than rutile? - Model studies on epitaxial $TiO_2$ films", *Sci. Rep.*, **4** (2014) 1–8.
22. S. Farrokhpay, "A review of polymeric dispersant stabilisation of titania pigment", *Adv. Colloid Interface Sci.*, **151** (2009) 24–32.
23. F.A. Grant, "Properties of rutile (titanium dioxide)", *Rev. Mod. Phys.*, **31** (1959) 646–674.
24. G. Liu, Z. Chen, C. Dong, Y. Zhao, F. Li, G. Q. Lu, H.-M. Cheng, "Visible light photocatalyst: iodine-doped mesoporous titania with a bicrystalline framework", *J. Phys. Chem. B*, **110** (2006) 20823–20828.
25. E.K. Rajashekhar, G.L. Devi, "Polymorphic phase transformation of Degussa P25 $TiO_2$ by the chelation of diaminopyridine on $TiO_6$ ratio on the photocatalytic activity", *J. Mol. Catal. A*, **374-375** (2013) 12–21.
26. B. Ohtani, O.O. Prieto-Mahaney, D. Li, R. Abe, "What is Degussa (Evonik) P25? Crystalline composition analysis, reconstruction from isolated pure particles and photocatalytic activity test", *J. Photochem. Photobiol. A*, **216** (2010) 179–182.
27. T. Ohno, K. Sarukawa, K. Tokieda, M. Matsumura, "Morphology of a $TiO_2$ photocatalyst (Degussa, P-25) consisting of anatase and rutile crystalline phases", *J. Catal.*, **203** (2001) 82–86.
28. F. Dachille, P.Y. Simons, R. Roy, "Pressure-temperature studies of anatase, brookite, rutile and $TiO_2$-II", *Am. Mineral.*, **53** (1968) 1929–1939.
29. A.A. Gribb, J.F. Banfield, "Particle size effects on transformation kinetics and phase stability in nanocrystalline $TiO_2$", *Am. Mineral.*, **82** (1997) 717–728.
30. H. Zhang, J.F. Banfield, "Thermodinamic analysis of phase stability of nanocrystalline titania", *J. Mater. Chem.*, **8** (1998) 2073–2076.
31. B. Gilbert, H. Zhang, F. Huang, M.P. Finnegan, G.A. Waychunas, J.F. Bamfield, "Special phase transformation and crystal growth pathways observed in nanoparticles", *Geochem. Trans.*, **4** (2003) 20–27.
32. H. Zhang, J.F. Banfield, "New kinetic model for the nanocrystalline anatase-to-rutile transformation revealing rate dependence on number of particles", *Am. Mineral.*, **84** (1999) 528–535.
33. H. Zhang, J.F. Banfield, "Understanding polymorphic phase transformation behaviour during growth of nanocrystalline aggregates: insights from $TiO_2$", *J. Phys. Chem. B*, **104** (2000) 3481–3487.
34. K.P. Kumar, "Growth of rutile crystallites during the initial stage of anatase-to-rutile transformation in pure titania and in titania-alumina nanocomposites", *Scr. Mater.*, **32** (1995) 873–877.
35. A. Navrotsky, O.J. Kleppa, "Enthalpy of the anatase-rutile transformation", *J. Am. Ceram. Soc.*, **50** (1967) 626–630.
36. W. Li, C. Ni, H. Lin, C.P. Huang, S. Ismat Shah, "Size dependence of thermal stability of $TiO_2$ nanoparticles", *J. Appl. Phys.*, **96** (2004) 6663–6668.
37. P. Galizia, C. Baldisserri, C. Galassi, "Microstructure development in novel titania-cobalt ferrite ceramic materials", *Ceram. Int.*, **42** (2016) 2634–2641.
38. P. Galizia, I.V. Ciuchi, D. Gardini, C. Baldisserri, C. Galassi, "Bilayer thick structures based on

$CoFe_2O_4/TiO_2$ composite and niobium-doped PZT obtained by electrophoretic deposition", *J. Eur. Ceram. Soc.*, **36** (2016) 373–380.
39. R.A. Spurr, H. Myers, "Quantitative analysis of anatase-rutile mixtures with an X-ray diffractometer", *Anal. Chem.*, **29** (1957) 760–762.
40. A.K. Datye, G. Riegel, J.R. Bolton, M. Huang, M.R. Prairie, "Microstructural characterization of a fumed titanium dioxide photocatalyst", *J. Solid State Chem.*, **115** (1995) 236–239.
41. H. Jensen, K.D. Joensen, J.-E. Jorgensen, J.S. Pedersen, E.G. Sogaard, "Characterization of nanosized partly crystalline photocatalysts", *J. Nanopart. Res.*, **6** (2004) 519–526.
42. R.L. Penn, J.F. Banfield, "Oriented attachment and growth, twinning, polytypism, and formation of metastable phases: insights from nanocrystalline $TiO_2$", *Am. Mineral.*, **83** (1998) 1077–1082.